Eur Biophys J (2008) 37:345–358
DOI 10.1007/s00249-008-0264-5

REVIEW

Development of phase plates for electron microscopes and their biological application

Kuniaki Nagayama

Received: 1 October 2007 / Revised: 24 December 2007 / Accepted: 8 January 2008 / Published online: 8 February 2008

Abstract After slow progress in the efforts to develop phase plates for electron microscopes, functional phase plates with thin carbon films have recently been reported. An electron microscope enhanced with thin-film phase plates has practical advantages. It permits collecting high-contrast images of intact biological specimens without harsh and lengthy sample preparation, such as fixation, dehydration, resin-embedding, staining and thin-sectioning. This report reviews the state of the art for phase plates in biological electron microscopy and focuses upon the conditions required for functional thin-film phase plates. The current disadvantages of thin-film phase plates are also addressed and potential solutions are proposed.

Keywords Electron microscope · Phase contrast · Phase plate · Thin-film · Cryomicroscopy · Zernike

Introduction

To visualize transparent materials, transmission electron microscopy (TEM) traditionally has employed a phase-contrast method, defocus phase contrast, that is commonly used in high-resolution studies of inorganic materials (Reimer 1997). Unfortunately, a fundamental flaw in the application of this method to biological specimens is the difficulty of reconciling contrast and resolution. One approach for surmounting this problem would be to employ a phase contrast method that utilizes phase plates, similar to the method used to visualize transparent objects by light microscopy. Theoretically, electron microscopy is compatible with three different types of phase plates (Boersch 1947): thin-film, electrostatic, and magnetic. However, designing functional phase plates have been an arduous process that has suffered from unavoidable technical obstacles such as the thin-film phase-plate charging and difficulties associated with micro-fabrication of electrostatic and magnetic phase plates. Recently, Nagayama et al. have overcome difficulties concerning to the thin-film phase plate and been fairly successful to obtain higher contrast images for unstained biological specimens (refer to a review by Nagayama 2005a).

This review reports the state of the art in functional phase plates that focuses on thin-film phase plates. First, this review describes the methodology of phase-contrast TEM with phase plates with the aid of simulated images. Second, it deals with recent studies on biological applications of phase-contrast TEM. Third, emerging technologies to overcome the obstacle of phase-plate charging and functional anti-static phase plates are reported. Next, I discuss electron loss, a disadvantage of thin-film phase plates. Last, I present the advanced phase-plate technologies to overcome the electron loss with elaborate designs of electrostatic and magnetic phase plates.

K. Nagayama (✉)
Department of Physiological Science, SOKENDAI,
Okazaki Institute for Integrative Bioscience and National Institute for Physiological Sciences,
National Institutes of Natural Sciences,
Okazaki 444-8787, Japan
e-mail: nagayama@nips.ac.jp

Methodology of phase plates in electron microscopy

The first phase visualization technique appeared at the end of the nineteenth century with Schlieren optics using the Foucault knife-edge, which half covered the back-focal plane of the objective lens. The Zernike phase

contrast (ZPC) (Zernike 1942) and the Smith/Nomarski differential interference contrast (DIC) (Smith 1947; Nomarski 1952) methods followed. Defocus phase contrast (DPC) was originally devised and developed by Scherzer for electron microscopy (Scherzer 1949). The extension of ZPC to electron microscopy has been attempted for some time but only very recently one approach has, using thin-film phase plates, been realized with substantial success (Danev and Nagayama 2001). This same group has also demonstrated a phase-plate version of DIC (Danev et al. 2002).

The visualization of phase objects can be described with a minimum microscopic-model that assumes only elastic scattering, coherent illumination with a plane wave incidence and phase objects that optically disturb incident electron waves only in phase. The phase change produced in these phase objects are represented with a two-dimensional transparency function, $T(r) = e^{i\theta(r)}$, where $\theta(r)$ corresponds to a special variation of the phase retardance.

In electron microscopy, $\theta(r)$ may be related to the constituent atomic potential in the sample (Mott and Massey 1965):

$$\theta(r) = \sum \theta_k g_k(r - r_k) \quad (1)$$

where θ_k is the phase retardation factor associated with the potential of the kth atom and $g_k(r - r_k)$ describes the atom distribution.

The image formation process in TEM can be schematized as shown in Fig. 1a, where a minimal model based on the wave picture is illustrated. The corresponding wave optical abstraction can be mathematically formulated as shown in Fig. 1b. The formulation is nothing more than a mathematical interpretation of Abbe's notion for image formation in microscopy. Images are generated in two successive diffractions, where the diffraction is abstracted to a Fourier transform. In this scheme, phase plates are symbolized as a spatial filter that modulates diffracted electron waves in a

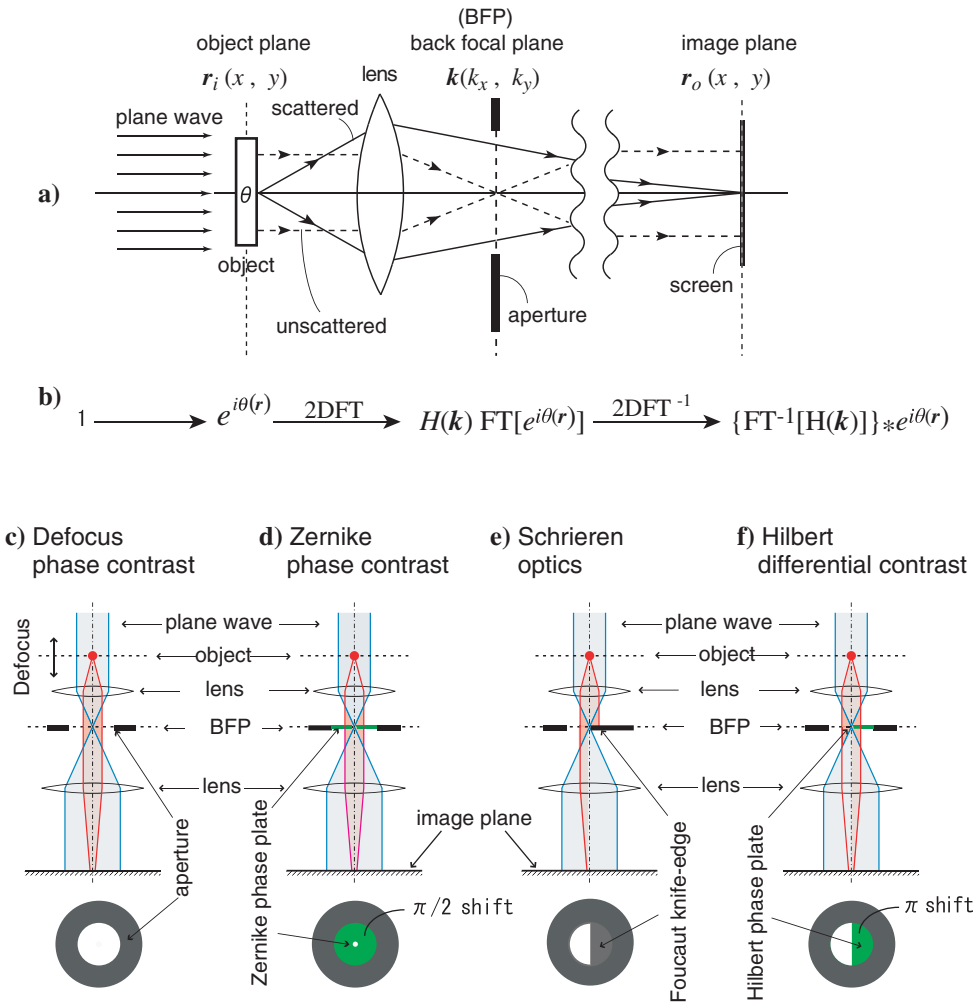

Fig. 1 Schematics describing the image formation process in a microscope. **a** A physical schematic using the wave optical picture for the transfer of light or electrons. **b** Corresponding mathematical formulation. *2D FT* two-dimensional Fourier transform, *FT[ ]* two-dimensional (2D) FT operation, $H(k)$ spatial filter, $2DFT^{-1}$ inverse 2DFT, $FT^{-1}[\ ]$ inverse 2DFT operation, and * convolution. **c** A spatial filter schematic for the defocus phase contrast (DPC). **d** A spatial filter schematic for the Zenike phase contrast (ZPC). **e** A spatial filter schematic for Schlieren optics (SO) or single-sideband imaging (SSI). **f** A spatial filter schematic for Hilbert differential contrast (HDC)

frequency-dependent manner at the back focal plane of the objective lens.

With this minimum microscopic model, the principle of phase contrast for pure phase objects is simply described as:

1. The two-dimensional wave property is described by $e^{i\theta(r)}$, the exit-wave function at the exit plane beyond the phase objects. The intensity of such an exit-wave function is constant because Eq. 2 is a mathematical abstraction representing transparency of phase objects.

$$\left|e^{i\theta(r)}\right|^2 = 1 \tag{2}$$

2. Phase contrast microscopy generates the phase contrast with a spatial filter, $H(k)$, as

$$\left|\left\{FT^{-1}[H(k)]\right\} * e^{i\theta(r)}\right|^2 \neq 1 \quad (*\text{represents convolution}) \tag{3}$$

Formulation II represents the broadest sense of the definition for phase contrast. According to the choice of spatial filters, four types of schemes for phase plates can be considered as shown in Fig. 1c–d.

The typical phase contrast, ZPC, and the oldest and most illuminative scheme, Schlieren optics, that is known in the electron microscopist community as single-sideband imaging, both can be expressed as spatial filters. However, the Smith/Nomarski phase contrast, DIC, does not appear to be included in the simplest model shown in Fig. 1, as it employs a design to insert a birefrigent optical device even before the objective lens. This methodological discord has been recently removed with a novel scheme that includes a half-plane $\lambda/2$ phase-plate inserted at the back-focal-plane after the objective lens as a spatial filter to retard the electron waves by π (Danev et al. 2002). This setup is termed Hilbert differential contrast (Danev and Nagayama 2004).

Standard textbooks of optics instruct (Born and Wolf 1999) that what is transferred in optical devices in the case of incoherent illumination is not the innate wave (the wave function itself), but the intensity or the irradiance of the wave (squared wave function). Therefore, incoherent illumination automatically eliminates any type of phase contrast because the exit wave function, $e^{i\theta(r)}$, has a uniform intensity of one ($|e^{i\theta(r)}|^2 = 1$). In contrast, the minimum model assumes a coherent illumination that guarantees the transfer of the exit wave function itself rather than the intensity that lacks phase information.

To illustrate the phase contrast principle as formulated in Eq. 3, simulated images were computed for an imaginative phase object, Red Fuji, by Hokusai. Four schemes with different spatial filters were chosen for the simulation: defocus phase contrast (DPC), Zernike phase contrast (ZPC), Schlieren optics (SO) or single-sideband imaging (SSI), and Hilbert differential contrast (HDC). To pinpoint the essence of the phase contrast in this simulation, two assumptions were included. First, the image was a simulation for an ideal microscope that does not possess aberration. Second, the phase plates were ideal and recovered spatial frequencies as close as possible to zero. The size scale of Red Fuji was reduced by a factor of 10^{10} for this simulation, and the darkest feature was assumed to correspond to a phase change of $\pi/4$.

Based on the general formalism given in Fig. 1b, the applicability of phase contrast is not limited to weak phase objects ($|\theta| << 1$). This is illustrated by using a few figures of images obtained with the computer simulation in Fig. 2. Throughout the simulation no assumptions were made for weak phase objects. Instead, the image formation provided in Fig. 1b was strictly followed. Images corresponding to $\left|\left\{FT^{-1}[H(k)]\right\} * e^{i\theta(r)}\right|^2$ were calculated for DPC. For ZPC, save for the 0th order diffraction ($k = 0$), all the frequency components corresponding to FT [$e^{i\theta(r)}$] were multiplied by $-i$ (this is the mathematical expression for the $\pi/2$ phase shift for scattered electrons) and the same procedure as for DPC was employed. In actual ZPC-TEM, the assumed ideal condition cannot be fulfilled. The consequence is that the recovery of phase contrast corresponding to the lower frequencies, around $k = 0$, is not attained. This results in the problem of the different appearance of the image contrast.

Figure 2 illustrates simulated images for Red Fuji with variations in the phase contrast associated with a specific filter condition.

The simulation reveals that the defocus amount affects the appearance of the image (compare Fig. 2c–f).

The other pair of phase contrast images is single-sideband imaging (SSI) and Hilbert differential contrast (HDC) (Fig. 2g, h). They illustrate topographical images for Red Fuji obtained with a Foucault knife-edge for SSI and a half-plane $\lambda/2$ phase plate (Hilbert phase plate) for HDC. However, the HDC simulation appears to possess a contrast that is twice that of SSI. This can be deduced from simple arithmetic as the Foucault knife-edge interrupts exactly half of the total electrons. The higher contrast of both images is also associated with the cosine-CTF, similar to ZPC (Danev et al. 2002).

The next issue is how to practically realize excellent images obtainable through phase plates as revealed by the simulation.

Application of thin-film phase plates to biological samples

All of the experiments reported in this section were conducted with a 300 kV TEM system. The specifications of this system are provided elsewhere (Nagayama 2005a).

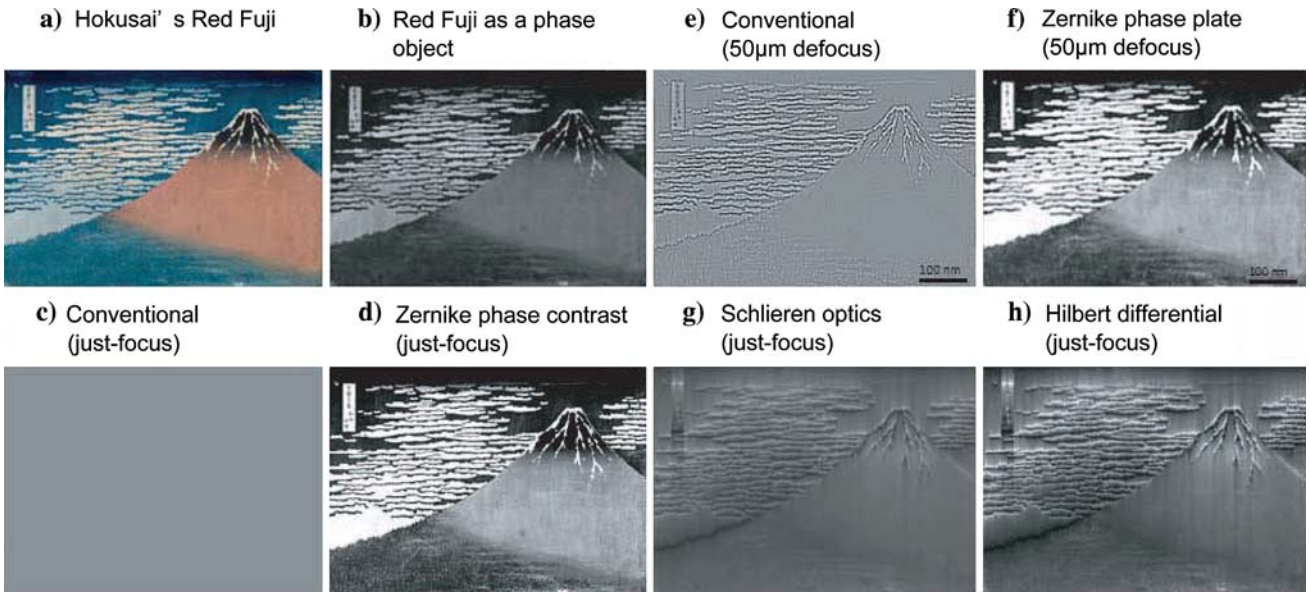

Fig. 2 TEM image simulations with various spatial filters, for a 10^{-10}-fold demagnified version of Red Fuji, by varying the defocus condition with a k_{max} aperture. The original Red Fuji (**a**) converted to a *black and white picture* (refer to **b**) and the *black* and *white* Fuji assumed to be a phase object by setting the *full black* to be a phase shift by $\pi/4$. The maximum aperture size (k_{max}) corresponds to the Nyquist frequency. **a** Original Red Fuji by Hokusai. **b** A *black* and *white* version converted from the *full-color* Red Fuji. **c** A conventional image with just-focus for the phase-object-converted Red Fuji. **d** A ZPC image with just-focus for the phase-object-converted Red Fuji. **e** A conventional image with a deep defocus of 50 μm for the phase-object-converted Red Fuji. **f** A ZPC image with a deep defocus of 50 μm for the phase-object-converted Red Fuji. **g** A Schlieren optics image with just-focus for the phase-object-converted Red Fuji. **h** A HDC image with just-focus for the phase-object-converted Red Fuji. Edges of the knife-edge and Hilbert phase plate are horizontally aligned to the orientation of Red Fuji in the image

Cryo-technique

Sample preparation has always been one of the most difficult and critical issues in applying TEM to biological samples. There are three major difficulties inherent in biological specimens: (1) they are best preserved in aqueous media that is inappropriate for vacuum conditions, (2) they consist of light elements (H, C, N, and O) that weakly diffract electron waves, and (3) the morphology is complex. Tremendous effort has been dedicated to resolving these difficulties and the development of biological TEM includes a long history of innovations in sample preparation.

The standard method for preparing samples is extraordinarily useful because it allows for easy handling with a series of procedures for fixation, dehydration, resin-embedding, staining, and thin-sectioning.

The problems inherent to the traditional approach for sample preparation have nearly all been solved by cryo-techniques. Rapidly frozen ice-embedded specimens provide reliable micrographs that reflect the intrinsic internal structures of biological samples (Fernandez-Moran 1960; Heuser et al. 1979; Van Harreveld and Crowell 1964) because these samples are considered to be free from artifacts induced by the standard method of preparation.

Application of ZPC-TEM to protein structures

In ZPC with Zernike phase plates, the finite size of the central hole limits the recoverable lower spatial frequencies. For example, for a 300 kV TEM system with a Zernike phase plate with a hole size of 0.5 μm in diameter, this value is about 0.02 nm^{-1} ($\sim$50 nm). Given this limitation, one application of ZPC-TEM is structural studies of proteins and protein–lipid structures with geometries at or below 100 nm.

Figure 3a and b illustrates the differences between a conventional and a ZPC image for the chaperonin protein GroEL. Several competing groups intensively pursued the 3D reconstruction of this protein with TEM single-particle analysis (Ludtke et al. 2004; Ranson et al. 2001; Saibil 2006; Stagg et al. 2006). The advantage of ZPC is clearly visible (Fig. 3b). Figure 3a provides a ZPC image corresponding to the simulation in Fig. 2a and Fig. 3b corresponds to the simulation in Fig. 2e. The most difficult component of the single particle analysis when performed with the conventional approach is the first step, selecting the images that correspond to protein molecules. Individual protein molecules must be identified from noisy raw images that usually have very poor contrast, as shown in Fig. 3b. Typical examples for sine and cosine CTFs that characterize

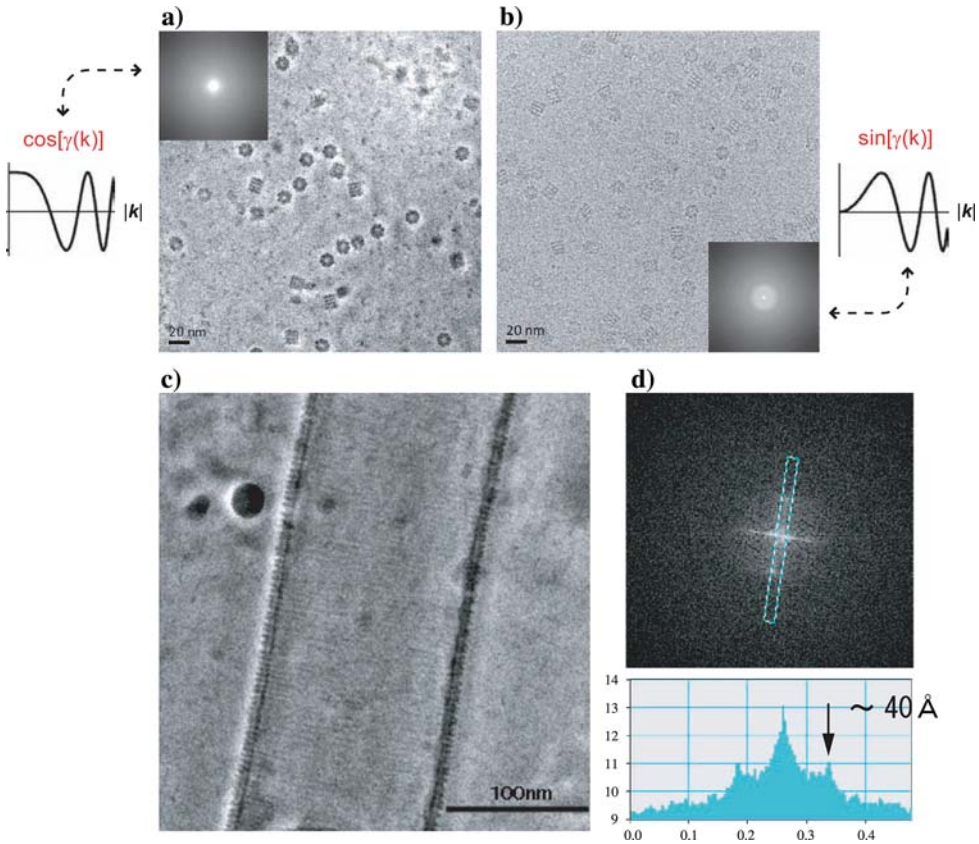

Fig. 3 TEM images (300 kV) for protein systems. **a** A ZPC image for an ice-embedded sample of GroEL. The inset is a diffractogram obtained by Fourier-transform of the image. A typical cosine CTF is shown. This can be experimentally determined with the kind of diffractogram shown in the inset. **b** A conventional image for an ice-embedded sample of GroEL. The inset is a diffractogram obtained by Fourier-transform of the image. A typical sine CTF is shown. This can be experimentally determined with the kind of diffractogram shown in the inset. **c** A ZPC image for a tubulated membrane liposome wrapped by a polymeric protein fiber. **d** A diffractogram obtained from **c** and an associated Fourier spectrum extracted from the diffractogram (**c** and **d** are adopted from Shimada et al. 2007)

the frequency response appearing in the images with and without the ZPC phase plate are inserted in Fig. 3a and b. CTFs, which are functions defined in the Fourier or *k* space can be experimentally determined by analyzing diffractograms as shown in the inlets of Fig. 3a and b.

A comparative study of the 3D reconstructions for GroEL from images obtained with and without Zernike phase plates has been reported (Danev and Nagayama 2008).

Another example of how ZPC images can add decisive morphological information is provided in Fig. 3c and d. One unresolved issue regarding endocytosis is the determinant for the membrane invagination. Many researchers have proposed that specific proteins mediate this process. Images obtained by phase contrast cryo-TEM with a Zernike phase plate reveal that a recently discovered protein is associated with membrane invaginations (Shimada et al. 2007). Figure 3c shows a tubulated lipid membrane tightly wrapped by a filamentous polymer comprising a dimer of the protein, EFC/F-BA-domain. X-ray crystallographic studies have determined the structure of this protein and predicted that the spacing of the polymer wrapping around lipid is approximately 3.5 nm. This prediction is consistent with an image of the polymer surrounding the lipid, in which, the spacing determined by Fourier analysis was 4.0 nm (Fig. 3d).

Application of HDC-TEM to cells

The most striking application of HDC-TEM to biology is the phase contrast image of an entire cell in an ice-embedded state. These results were completely unexpected by researchers using biological TEM, as cells have been considered to be dense objects that require sectioning prior to imaging.

Cyanobacterial cells were the first to be imaged with HDC-TEM (Kaneko et al. 2005, 2006). The HDC-TEM image can display topographic features and appears similar to images obtained with differential interference contrast light microscopy (Danev et al. 2002). This high-contrast version of TEM corresponds to the simulation shown in Fig. 2h. HDC-TEM micrographs of an ice-embedded cyanobacterial whole cell are shown in Fig. 4a (Kaneko et al. 2007). Surrounded by smooth cell walls, the thylakoid membranes and carboxysomes are visible (refer to Fig. 4d, e). These structural features were confirmed by comparing HDC-TEM micrographs to conventional TEM images of ultrathin sections of chemically fixed and resin-embedded cyanobacteria (Fig. 4c). Large electron dense spherical polyphosphate bodies are prominent structures in the HDC-TEM images (arrow in Fig. 4c). These structures cannot be observed in images obtained following the standard preparation because of the difficulties associated with

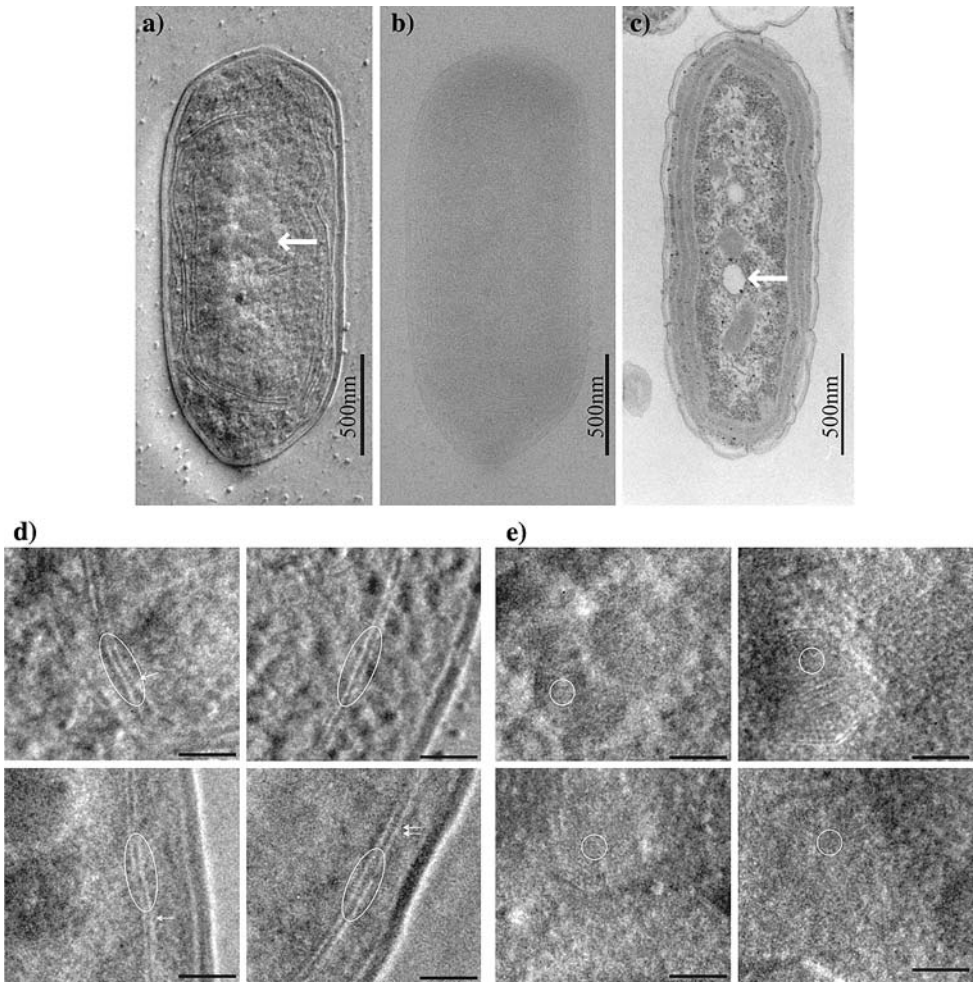

Fig. 4 TEM images (300 kV) of a vitrified cyanobacterial cell. **a** A HDC just-focused image of an ice-embedded cyanobacterial whole cell. The polyphosphate bodies (*arrow*) are prominent among detailed ultrastructures. **b** A conventional TEM image of an ice-embedded cyanbacterial cell for the same view field as in a wih, a defocus setting of 15 μm. **c** A 100 kV conventional TEM image of a chemically fixed, resin-embedded, and thin-sectioned cell stained with uranyl acetate and lead citrate. Polyphosphate bodies are lost during the preparation process. This leaves an empty hole in the section (*arrow*). **d** Thylakoid membranes identified in the HDC images of cyanobacterial cells. **e** Carboxyzomes identified in the HDC images of cyanobacterial cells (adopted from Kaneko et al. 2005)

preserving them. These polyphosphate bodies appear to shrink considerably during chemical fixation and dehydration, leaving spaces around them. Consequently, they are often lost during ultrathin sectioning. They usually appear as empty holes in ultrathin sections (arrow in Fig. 4b).

Functional thin-film phase plates

In the application of SEM to biological materials, charging of objects has always been a fundamental issue. The same holds true for phase plates. Static charges induced in contaminants on the surface of the phase-plate carbon-film by electron bombardment (refer to Fig. 5a) may be caused by ionization of atoms and behave as micro-lenses that inevitably affect the transfer of electron waves and adversely affect the resultant images.

Figure 5a shows a schematic of how charged particles contaminate the surface of a ZPC phase plate. Figure 5b shows a corresponding CTF patterns obtained for a thin-film made of amorphous carbon with and without a ZPC phase plate. One-dimentional power spectra were obtained by rotationally averaging and background-subtracting the diffractograms, as shown in the inlets on Fig. 3a and b. A rough comparison of the CTF amplitudes reveals about a roughly 20% reduction in the signal of the phase-plated image. This indicates an electron loss in the thin-film phase plates. This concept will be more thoroughly discussed below as a future target for development. Theoretically, the two CTFs that correspond to the sine CTF and cosine CTF (as shown in Fig. 3a, b) should be complementary to a shift of $\pi/2$. However, because of charging, the cosine CTF corresponding to the ZPC is distorted. Figure 5c plots the phases extracted from the two CTFs by fitting the extreme positions of the CTFs shown in Fig. 5b. The phase of the sine CTF matches the theoretical model. The interpolated values for the sine CTF are then subtracted from those of the cosine CTF, calculating the phase retardation associated with the phase plate. In this case, the cosine CTF begins with a negative value

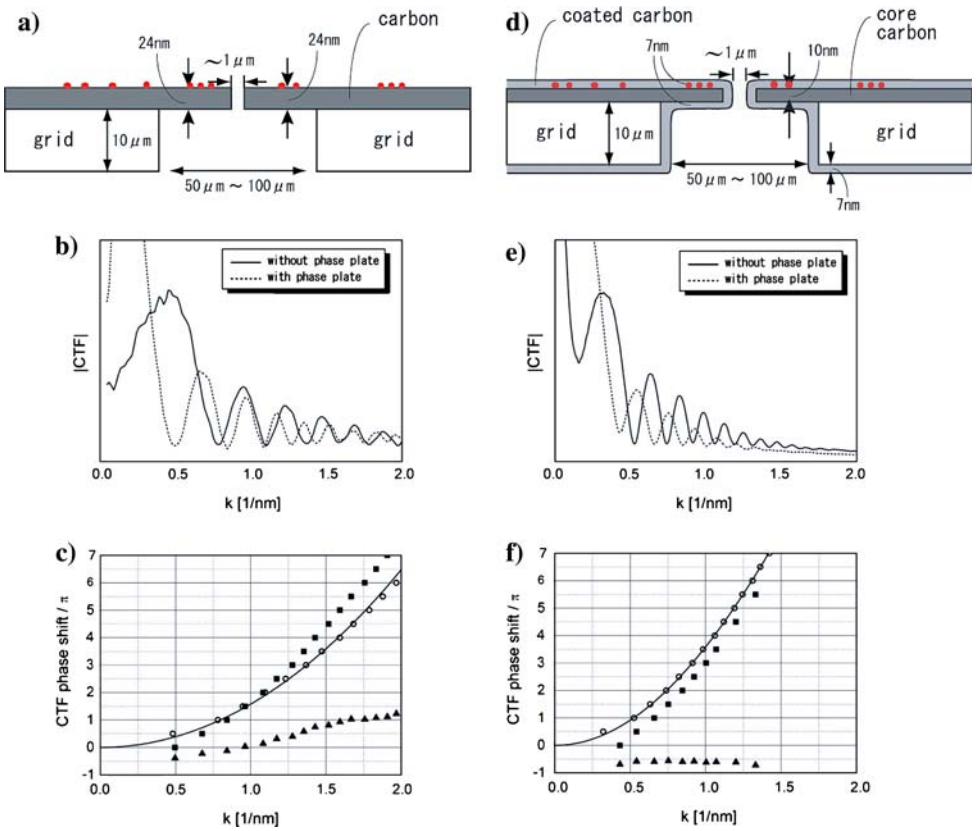

Fig. 5 Methods to resolve the charging in the thin-film phase plates. **a** Typical design for a Zernike phase plate made of carbon film for an acceleration voltage of 120 kV. Contaminants (*red dots*) sitting on the plate surface are responsible for the emergence of an electrostatic potential once charged. **b** Rotationally averaged profiles of diffractograms obtained for a standard sample with and without a Zernike phase plate as shown in (**b**). **c** CTF phase extracted by fitting the extreme positions in the profiles in (**b**). **d** Difference between the two CTF phases (*open circle* without phase plate, *filled square*: with phase plate) provides the phase retardation (*filled triangle*) introduced by the phase plate. **d** Three-layered carbon film designed to avoid the charging effect in a Zernike phase plate. Contaminants are wrapped by a conductive carbon coat to shield the electrostatic potential. **e** Rotationally averaged profiles of diffractograms obtained for a standard sample with and without a Zernike phase plate as shown in **d**. **f** CTF phase extracted by fitting the extreme positions in the profiles in **e**. Difference between the two CTF phases (*open circle* without phase plate, *filled square* with phase plate) provides the phase retardation (*filled triangle*) introduced by the phase plate (adopted from Nagayama 2005a)

(-0.4π at $k = 0.5$ nm^{-1}) that gradually increases along k. This behavior is similar to overfocusing and a result of the presence of positive charges around the center of the phase plate (Danov et al. 2001, 2002).

TEM pioneers noted that contamination on the surface of phase plates by insulating materials was the source of the charge (Faget et al. 1962; Badde and Reimer 1970; Balossier and Bonnet 1981; Krawkow and Siegel 1975). The phase plate itself is not charged when made of a conducting material such as carbon. Several years efforts for hunting after actual origins of contaminants made by Nagayama and colleagues, have demonstrated that there are three sources for charge contamination: organic materials, metal oxides, and inorganic materials (refer to a review by Nagayama 2005a).

Organic molecules have long been recognized as the major source of charge contamination. Several methods have been proposed to remove contamination, including using oil-free vacuum systems for the phase-plate fabrication, rinsing of phase plates with organic solvents, and heating, ultraviolet (UV) irradiation, ion sputtering, or electron-preirradiation of the phase plates. Among these latter potential remedies, heating seems to be most effective. However, organic-free preparations of phase plates are easily contaminated inside the TEM column with organic materials evaporated from biological samples during electron bombardment. Accordingly, continuously heating the phase plate inside the TEM column was proposed and implemented decades ago (Sieber 1974).

Metal oxides are a prevalent source for charging and the major reason why phase plates are fabricated from carbon. Nonetheless, metal-oxide contamination during the deposition process of carbon films for phase plates, with a

vacuum evaporator, for example, must be carefully avoided by using metal-oxide-free devices. The best materials for these devices are glass, stainless steel, and carbon. Another source for metal oxide contamination of phase plates is the drilling of a hole in the plate by focused-ion-beam (FIB) fabrication. Gallium, the ion source for FIB, may remain on or in the phase plate after the FIB fabrication and converted to gallium oxide.

Inorganic contamination, particularly from a mica surface, is a source of charge that is nearly impossible to avoid. During the peeling process, a separation crack typically develops at the interface between the carbon film and the mica, but occasionally the crack approaches the mica-layers gap, which can lead to mica-flakes attaching to the carbon film. Pessimistically, we have concluded from our charge-origin studies that the contamination during the preparation process cannot be avoided.

Thus, to solve the phase-plate issue, we employed an old idea, electrostatic shielding. The charge-induced potential can be shielded by coating with conductive material such as carbon. The core of this solution is that the presence of charge and the charge effect are separable. In the final step of phase-plate production, both sides of the phase plate, likely contaminated with organic materials, metal oxides, or inorganic materials, are coated with carbon with a vacuum evaporator. The carbon wrapping over the entire phase plate must remain clean. Consequently, once grounded, the electrostatic potential arising from charges is eliminated (refer to contaminants wrapped by a carbon coat in Fig. 5d). The schematic of a three-layered phase plate constructed with a carbon coating finish is shown in Fig. 5d. As shown in the CTF phase in Fig. 5e, the phase retardation due to the $\pi/2$ phase plate is confirmed by a flat curve that is almost free from the charging effect. This three-layered amorphous-carbon phase-plate has been a key breakthrough in the development of a functional phase plate.

Other technological advances that are contributing to adapting phase-plate TEM for routine use on biological specimens are: (1) a multi-hole phase-plate grid made from molybdenum (there are 25 holes usable as phase-plate apertures), (2) a heating phase-plate holder similar to a conventional specimen holder, (3) microfabrication of phase plates with a precision of 0.05 μm with a focused ion beam apparatus, (4) a transfer-lens doublet inserted between the objective lens and the heating phase-plate holder to relay the backfocal plane immediately below the objective to a distant position, and (5) a goniometer to precisely align the phase-plate hole with the optical axis.

A dedicated phase-plated TEM assembled with these components has been reported (Hosokawa et al. 2005).

Electron loss in thin-film phase-plates

Electron loss by the phase plate

One of the disadvantages in using thin-film phase-plates is electron loss due to electron scattering by the plate (Danev and Nagayama 2001). Plates are fabricated with carbon films because heavy elements, such as metals, cause greater electron loss. To evaluate the effect of electron loss, the power spectra of the diffractograms between images taken with and without phase plates have been compared.

A frequency dependent index, $G(k)$ (gain), estimates the power-spectral gain yielded by a phase plate. It is defined as the ratio of the circular integration for the diffractograms obtained with and without phase plates. Figure 6a provides the calculation for $G(k)$ (Nagayama 2005a).

In the case of negatively stained ferritin images taken with and without a Zernike phase plate (Danev and Nagayama 2001), gain $G(k)$ in the low-frequency region is remarkable in every defocus condition employed. Particularly in the near focus condition (the upper most row in Fig. 6b), the gain is extraordinarily large, approximately 15, in the lower frequency region. The gain decreases when the defocus for the conventional image deepens. This is the expected result as the defocus phase contrast becomes higher when the defocusing is deeper.

In the case of ice-embedded cyanobacterial micrographs taken with a Hilbert phase plate, the gain is also remarkable in the lower frequency region, but an intensity loss is visible in the higher frequency region ($k > 0.1$ nm^{-1}) (the fourth row trace in Fig. 6b). The HDC method appears to specifically favor the recovery of lower frequency components since it allows us to adjust the incidence cross over that determines the origin of the spatial frequency at the diffraction (k–) space as close as possible to the edge of the half-plane phase plate. The recovery of lower frequency components with HDC is clearly shown as 0.02 nm^{-1}, that is the lower bound of the frequency in the gain curve $G(k)$ shown in the bottom right end of Fig. 6b.

A particular frequency that gives $G(k) = 1$ (no gain and no loss) is the point where the contrast enhancement due to the phase-plate offsets the contrast reduction. As previously mentioned, the gain profile of $G(k)$ depends on the defocus setting used for conventional TEM. Contrast enhancement due to a deep defocus is clearly reflected in the gain $G(k)$ that is obtained by comparing the near focus Zernike and the deep-defocus conventional (see the third row in Fig. 6b), where the zero crossing point is shifted to the very low-frequency region. This deep defocus effect is also evident in comparing the Hilbert and the conventional

a)

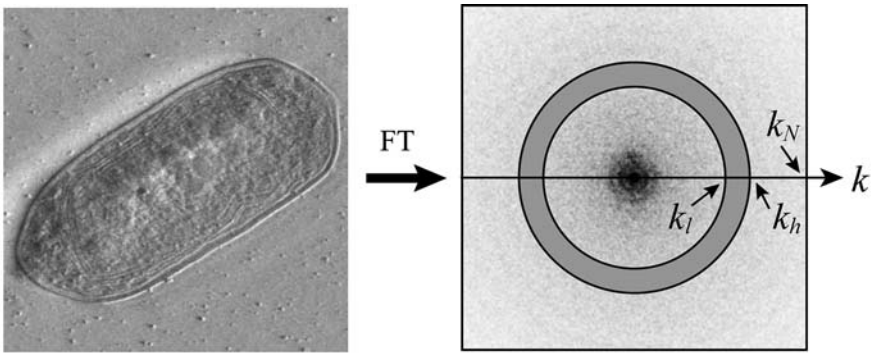

b)

	Material source	Image source $p_1(r)$	Image source $p_2(r)$	Δk $(=k_h-k_l)$	k_N	Gain profile ($G(k)$)
Zernike	Ferritin	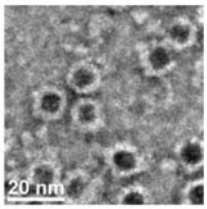	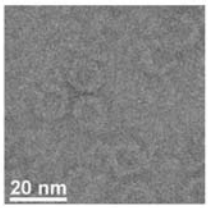	0.1 nm^{-1}	2 nm^{-1}	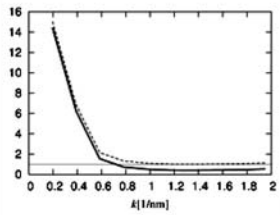
		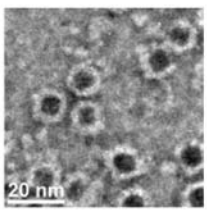	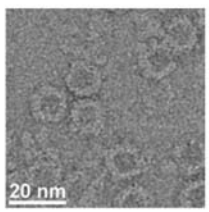	0.1 nm^{-1}	2 nm^{-1}	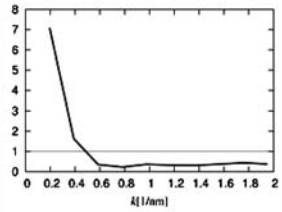
		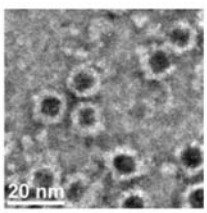	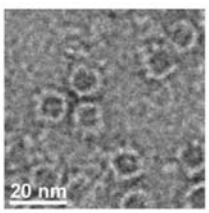	0.1 nm^{-1}	2 nm^{-1}	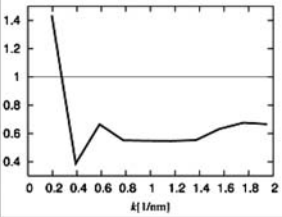
Hilbert	Cyanobacteria	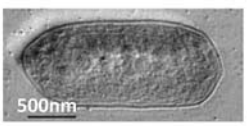	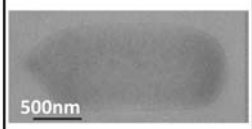	0.03 nm^{-1}	0.25 nm^{-1}	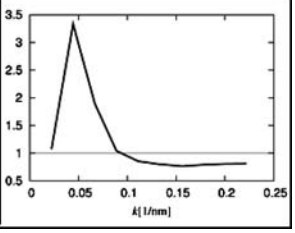

Fig. 6 Gain profiles obtained by comparing two corresponding images taken by phase contrast TEM with a Zernike or Hilbert phase plate and without a phase plate. **a** Schematics to illustrate the procedure to calculate the gain profile, $G(k)$. **b** Gain profiles obtained for the images taken with ZPC- or HDC-TEM. A *broken line* shown in the gain profile of the most upper trace is a putative profile if no loss of electrons is realized. Defocus values for Zernike and conventional images (top to down) of ferritin are 0, 0.13, 0.54, and 2.55 μm, respectively. Defocus values for Hilbert and conventional images of cyanobacteria are 0 and 15 μm, respectively (adopted from Nagayama 2005a)

contrast for cyanobacteria (see the fourth row in Fig. 6b) where the zero crossing occurs at a frequency around 0.1 nm^{-1}. It should be noted that an underfocus of 15 μm was used for conventional TEM imaging for cyanobacteria in order to maximize the image contrast (corresponding to the simulation shown in Fig. 2e).

There are several potential reasons for the contrast reduction in higher frequencies: (1) loss of coherent electrons by inelastic scattering, (2) diffuse scattering of elastic components by the ragged surface of phase plates, (3) exacerbated charging effect in the higher frequency region, and (4) the lowered optimum cut-off for the cosine CTF.

Overall, our 300 kV phase-contrast TEM with an aid of phase-plates enhances information, particularly in the frequency range smaller than 0.3 nm^{-1}.

Elaborate phase plates

Although the effectiveness of phase plates for recovering phase contrast was initially demonstrated with light microscopy, the idea of a Zernike phase plate for electron microscopy was proposed concurrently (Boersch 1947). In the pioneering work of Boersch, he proposed a few different options for phase plates that are shown in Fig. 7a. The concept of thin-film phase-plates was subsequently reinforced by a Japanese group employing collodion films or carbon films as phase plates (Kanaya et al. 1958).

Nevertheless, the contrast improvement has not been satisfactory save for recent successful results presented by Nagayama et al. with thin-film phase plates (Danev and Nagayama 2001; Danev et al. 2002; Danev and Nagayama

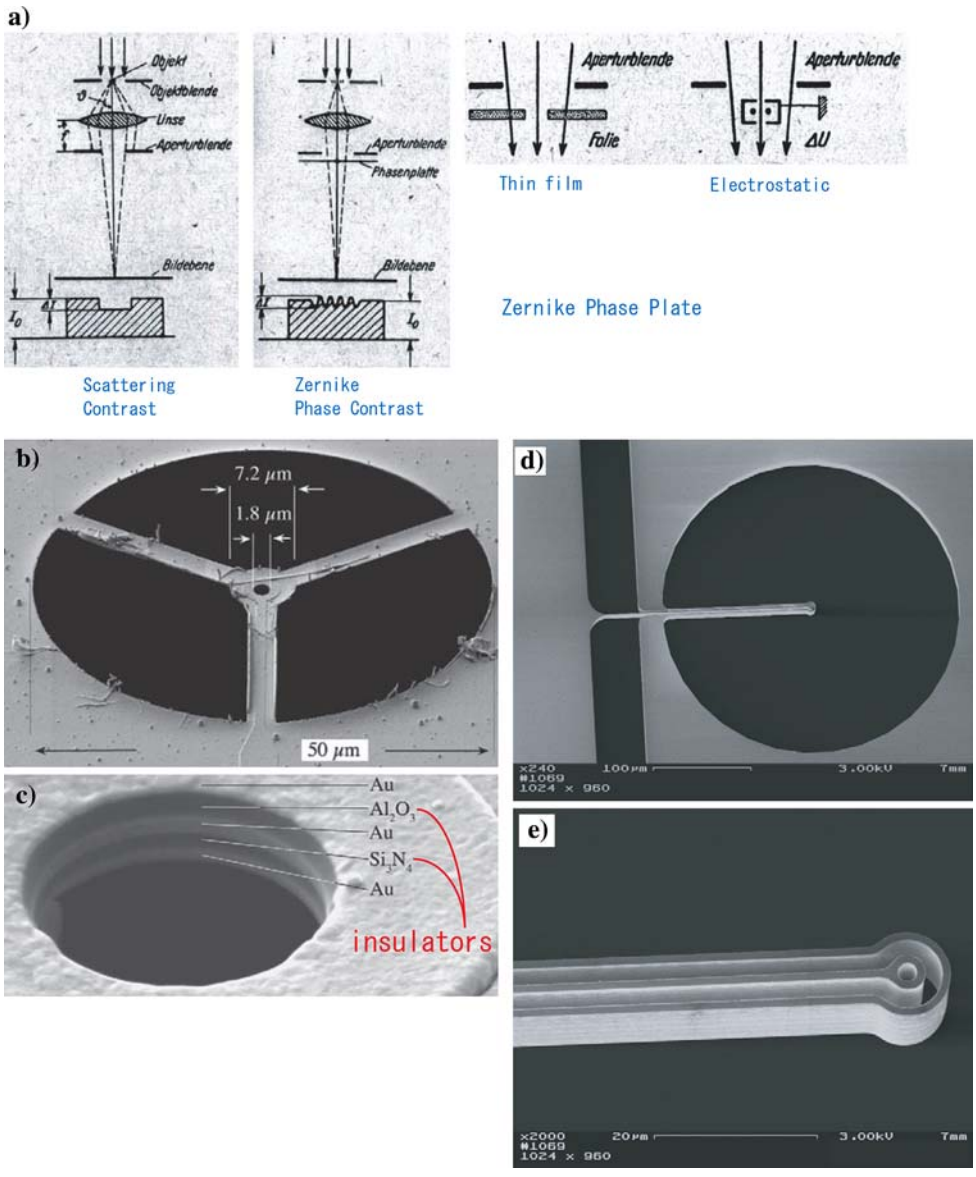

Fig. 7 Schematics and photos illustrating one type of elaborate phase plate using the electrostatic potential. **a** The first concept for an electrostatic phase plate proposed by Boersch (adopted from Boersch 1947). **b** An electrostatic phase plate made of a five-layered electrode supported by three spokes. **c** A close-up view of the central hole of the electrode (**b** and **c** are adopted from Majorovits et al. 2007). **d** An electrostatic phase plate made of a double-layered electrode supported by a single spoke. **e** A close-up view of the central hole of the electrode (**d** and **e** are adopted from Cambie et al. 2007)

2004; Kaneko et al. 2005; Nagayama 2005a; Kaneko et al. 2006, 2007; Shimada et al. 2007; Danev and Nagayama 2008). From 1958 until the end of the 1970s, various groups strived to make thin-film phase plates functional in ZPC or the equivalent (Faget et al. 1962; Unwin 1970; Badde and Reimer 1970; Johnson and Parsons 1973; Krawkow and Siegel 1975; Willash 1975; Balossier and Bonnet 1981).

A more sophisticated version of the Zernike phase plate containing a static ring electrode that can arbitrarily control the amount of phase shift (refer to the electrostatic plate in Fig. 7a) received attention from a Hitachi Co. group for their numerical work (Matumoto and Tonomura 1996). Recently, three groups reported that the electrostatic phase plate is technically tractable with the use of advanced microfabrication technology (Majorovits et al. 2007; Cambie et al. 2007; Huang et al. 2006). The Hitachi (Matsumoto) and Tsing-Hua (Huang) groups utilized two spokes to support a five-layered ring plate (three layers for electrodes and two layers for insulators) with an outer diameter (corresponding to the lowest bound of the spatial frequency recoverable) of 7 μm (Matsumoto) and 10 μm (Huang). In comparison, a Max Planck Institute group (Majorovits) used three spokes to support a five-layered ring electrode with an outer diameter of 7.2 μm (refer to Fig. 7b, c) and a Lawrence Berkeley Laboratory group (Cambie) employed one spoke to support a double-layered central electrode with an outer diameter of 10 μm (refer to Fig. 7d, e).

All three reports confirmed that the phase shift by $\pi/2$ corresponds to ZPC, but efficient phase contrast has yet to be reported in part due to the large outer diameter of the rings that is unable to recover lower frequency components (remember 0.5–1.0 μm in diameter for the hole of the Zernike phase plate developed by Nagayama et al. (Danev and Nagayama 2001, 2008)). In the design of these electrostatic phase plates, except for the Berkeley group, insulators are utilized to separate electrodes, which may induce charging as we experienced in the development of our thin-film phase plates.

In addition to electrostatic potential, another factor that can affect the electron wave phase is vector potential. The notion of whether a vector potential should be considered, a real physical entity or not, was at one time a central issue in physics. The Aharonov–Bohm (AB) effect emerged as a test to prove the reality of the vector potential (Aharonov and Bohm 1959). A decisive answer to this test was provided by the Hitachi group by using a small permalloy ring perfectly shielded with a superconducting material (Tonomura et al. 1986). In connection with this elegant result, the Hitachi group proposed to use a small permalloy ring to shift the phase of the incident electrons by $\pi/2$ as a patent application of a Zernike phase plate (Osakabe et al. 1985), which had an ideal design for the non-loss phase plate. Nevertheless, development to realize this design was not accomplished by this group. Similar difficulties may impede fabricating the electrostatic phase-plate shown in Fig. 7; namely, it is a delicate microfabrication and there are issues of how to support the magnetic ring.

Recently, the Nagayama group offered a solution to overcome this difficulty. They proposed applying the AB effect to the Hilbert phase plate (Nagayama 2005b; Yasuta et al. 2006). As shown in Fig. 8a2 and a4, a closed-loop magnet, when it confines the magnetic flux inside, generates a vector potential as expected by the AB effect and can differentiate the phase between electrons passing inside and outside of the loop. Adjustment of the confined magnetic-flux controls the extent of the phase change desired for HDC. If fabrication of the relatively large magnetic loop from ultrathin wire is difficult, the loop could be replaced with a straight long wire (bar) as shown in Fig. 8a3. One of the examples is a thin bar-magnet that is relatively easy to fabricate (Fig. 8a5).

Experimental results with a bar magnet (refer to Fig. 8a3) made of thin cobalt deposited onto a biprism that is normally utilized for electron holography are shown in Fig. 8b. The biprism wire made of platinum was slightly wider (800 nm width) than desirable for bar magnet appropriate for the Hilbert phase plate (π shift of electron waves could be generated with a saturated-state cobalt magnet having a cross section of about 2,000 nm^2, for example, 200 nm width × 10 nm thickness). In this preliminary experiment, the adjustment of the magnetic flux to yield the π shift was not achieved and hence the phase contrast could not be fully recovered. Despite that limitation, we were able to investigate the most crucial issue in the AB-Hilbert phase plate, electron loss.

The same index, $G(k)$, (as shown in Fig. 6) was calculated for pairs of TEM images taken with AB-Hilbert phase contrast (Fig. 8b1), deep defocus contrast (Fig. 8b2) and Shclieren optics (Fig. 8b3), and the just-focus conventional method (Fig. 8b4).

The gain curves shown in Fig. 8b5 must be compared with those in Fig. 8b7. The non-loss of the higher frequency components is evident with the AB-Hilbert phase contrast. The gain is not as high with the AB-Hilbert phase plate compared with the gain attained with the deep defocus contrast because of the incomplete π phase shift (compare curves of Fig. 8b5 and b6). However, this preliminary result obtained with the simplest version of the AB-Hilbert phase plate indicates that the approach is a promising candidate for the non-loss and non-charging

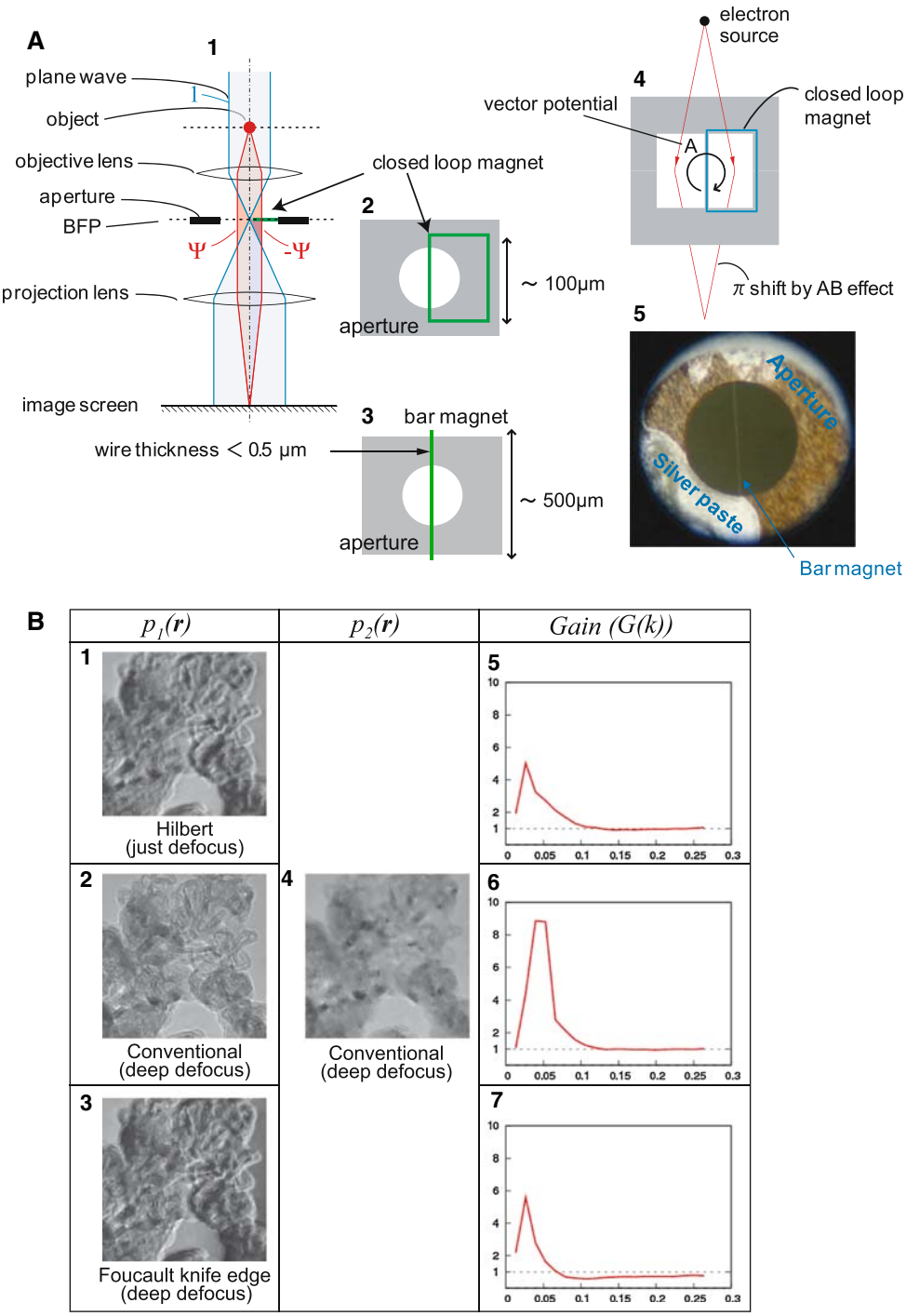

Fig. 8 Schematics and photos illustrating another type of elaborate phase plate using a thin-wire magnet to generate a vector potential. **a1** A schematic showing a microscope possessing a Hilbert phase plate at the back-focal-plane (BFP). **a2** A schematic of an AB-Hilbert phase plate using a closed-loop magnet. **a3** A schematic of an AB-Hilbert phase plates using a long-bar magnet. **a4** A schematic to illustrate a vector potential generated by a loop-magnet responsible for the phase change between electrons passing inside and outside. **a5** An example of a long-bar magnet (0.8 μm width × 2 mm length) made of cobalt thin-film deposited on a biprism. **b1** A 120 kV TEM image of a graphite sample taken with an AB-Hilbert phase plate as shown in **a5**. **b2** A 120 kV TEM image of a graphite sample taken with a deep defocus and without a phase plate (the same filed view as in **b1**). **b3** A 120 kV TEM image of a graphite sample taken with a deep defocus and a Foucault knife edge (the same view field as in **b1**). **b4** A 120 kV TEM image of a graphite sample taken with just focus and without a phase plate (the same view field as in **b1**). **b5** A gain profile comparing images of **b1** and **b4**. **b6** A gain profile comparing images of **b2** and **b4**. **b7** A gain profile comparing images of **b3** and **b4**

phase plate, the ultimate goal of our phase plate development.

Conclusions

Researchers in biological TEM tend to believe that conventional TEM can do the same job as phase-plate TEM for contrast enhancement. Hopefully, this review may provide quite a new aspect for the use of phase plates. However, overcoming skepticism regarding phase contrast remains difficult because, from a quantitative viewpoint, there are still drawbacks to phase-plate TEM, such as, electron loss and a lowered cut-off frequency. Surmounting these difficulties will require advances in phase-plate technology. For example, phase retardance due to matter (carbon) could be replaced by phase retardation due to non-matter such as electrostatic or vector potential described above.

In summary, the following conclusions can be reached:

1. Phase contrast with phase plates such as a Zernike phase plate or a Hilbert phase plate work as theory predicts within the limitation of practical technologies.
2. TEM images taken with an acceleration voltage of 300 kV can reach greater image contrast with phase plates.
3. HDC-TEM (300 kV) images are advantageous because they provide high-contrast images for unstained ice-embedded biological specimens of whole cells.
4. The long-standing issue of phase-plate charging can be resolved with a carbon-coating finish to shield the electrostatic potential arising from contaminant charge.
5. Heating the phase plate in situ without resting is quite effective to prolong the phase-plate life by avoiding the deposition of organic contaminants.
6. The two issues of electron loss due to thin-film phase-plates and the remaining charge effect, particularly in the high-frequency region, remain unresolved.

Acknowledgments I am grateful to the following collaborators for their contributions to the development and biological application of phase-contrast TEM with phase plates: *Development* Radostin Danev, Krassimir Danov, Rasmus Schroeder, Shozo Sugitani, Hiroshi Okawara, Toshiyuki Itoh, Toshikazu Honda, Toshiaki Suzuki, Yoshiyasu Harada, Yoshihiro Arai, Fumio Hosokawa, Sohei Motoki, and Kazuo Ishizuka; and *Applications* Koji Nitta, Yasuko Kaneko, Hitoshi Nakamoto, Atsushi Shimada, Shigeyuki Yokoyama, Nobuteru Usuda, Kimie Atsuzawa, Ayami Nakazawa, and Kiyokazu Kametani. This work was supported in part by a Grant-in-Aid for Creative Scientific Research (No. 13GS0016) from the Ministry of Education, Culture, Sports, Science, and Technology of Japan.

References

Aharonov Y, Bohm D (1959) Significance of electromagnetic potentials in the quantum theory. Phys Rev 115:485–491

Badde HG, Reimer L (1970) Der Einfluβ einer streuenden Phasenplatte auf das elektronen mikroskopische Bild. Z Naturforschg 25a:760–765

Balossier G, Bonnet N (1981) Use of elecrostatic phase plate in TEM. Transmission electron microscopy Improvement of phase and topographical contrast. Optik 58:361–376

Boersch H (1947) Über die Kontraste von Atomen in Electronenmikroskop. Z Naturforschg 2a:615–633

Born M, Wolf E (1999) Principle of optics, 7th edn. Cambridge University Press, Cambridge

Cambie R, Downing KH, Typke D, Glaeser RM, Jin J (2007) Design of a microfabricated, two-electrode phase-contrast element suitable for electron microscopy. Ultramicroscopy 107:329–339

Danev R, Nagayama K (2001) Transmission electron microscopy with Zernike phase plate. Ultramicroscopy 88:243–252

Danev R, Nagayama K (2004) Complex observation in electron microscopy. IV. Reconstruction of complex object wave from conventional and half plane phase plate image pair. J Phys Soc Jpn 73:2718–2724

Danev R, Nagayama K (2008) Single particle analysis based on Zernike phase contrast transmission electron microscopy. J Struc Biol 161:211–218

Danev R, Okawara H, Usuda N, Kametani K, Nagayama K (2002) A novel phase-contrast transmission electron microscopy producing high-contrast topographic images of weak objects. J Biol Phys 28:627–635

Danov K, Danev R, Nagayama K (2001) Electric charging of thin films measured using the contrast transfer function. Ultramicroscopy 87:45–54

Danov K, Danev R, Nagayama K (2002) Reconstruction of the electric charge density in thin films from the contrast transfer function measurements. Ultramicroscopy 90:85–95

Faget J, Fagot M, Ferre J, Fert C (1962) Microscopie electronique a contraste de phase. In: Proceedings of the 5th international congress electron microscopy A-7. Academic Press, New York

Fernandez-Moran H (1960) Low-temperature preparation techniques for electron microscopy of biological specimens based on rapid freezing with liquid helium II. Ann NY Acad Sci 85:689–713

Heuser JE, Reese TS, Dennis MJ, Jan Y, Jan L, Evans L (1979) Synaptic vesicle exocytosis captured by quick freezing and correlated with quantal transmitter release. J Cell Biol 81:275–300

Hosokawa F, Danev R, Arai Y, Nagayama K (2005) Transfer doublet and an elaborated phase plate holder for 120kV electron-phase microscope. J Electron Microsc 54:317–324

Huang SH, Wang WJ, Chang CS, Hwu YK, Kai JJ, Chen FR (2006) The fabrication and application of Zernike electrostatic phase plate. J Electron Mirosc 55:273–280

Johnson H, Parsons D (1973) Enhanced contrast in electron microscopy of unstained biological material. J Microsc 98:1–17

Kanaya K, Kawakatsu H, Ito K, Yotsumoto H (1958) Experiment on the electron phase microscope. J Appl Phys 29:1046–1049

Kaneko Y, Danev R, Nitta K, Nagayama K (2005) In vivo subcellular ultrastructures recognized with Hilbert-differential-contrast transmission electron microscopy. J Electron Microsc 54:79–84

Kaneko Y, Danev R, Nagayama K, Nakamoto H (2006) Intact carboxysome in a cyanobacterial cell visualized by Hilbert differential contrast transmission electron microscopy. J Bacteriol 188:805–808

Kaneko Y, Nitta K, Nagayama K (2007) Observation of in vivo DNA in ice embedded whole cyanobacterial cells by Hilbert differential contrast transmission electron microscopy (HDC-TEM). Plasma Fusion Res 54:79–85

Krawkow W, Siegel BM (1975) Phase contrast in electron microscope images with an electrostatic phase plate. Optik 42:245–268

Ludtke SJ, Chen DH, Song JL, Chuang DT, Chiu W (2004) Seeing GroEL at 6Å resolution by single particle electron cryomicroscopy. Structure 12:1129–1136

Majorovits E, Barton B, Schultheiß K, Perez-Willard F, Gerthsen D, Schröder RR (2007) Optimizing phase contrast in transmission electron microscopy with an electrostatic (Boersch) phase plate. Ultramicroscopy 107:213–226

Matumoto T, Tonomura A (1996) The phase constancy of electron waves traveling through Boersch's electrostatic phase plate. Ultramicroscopy 63:5–10

Mott NF, Massey HSW (1965) The theory of atomic collisions, 3rd edn. Clarendon Press, Oxford

Nagayama K (2005a) Phase contrast enhancement with phase plates in electron microscopy. Ad Imaging Electr Phys 138:69–146

Nagayama K (2005b) A phase plate for electron microscopes and its fabrication method (in Japanese), JPN-patent application, Tokugan 2005–321402

Nomarski G (1952) Interferométre á polarization, French patent 1.059.123

Osakabe N, Nomura S, Matsuda T, Endo J (1985) Phase contrast electron microscope, JPN-patent application, Tokugan 1985–7048 (in Japanese)

Ranson NA, Farr GW, Roseman AM, Gowen B, Fenton WA, Horwich AL, Saibil HR (2001) ATP-bound states of GroEL captured by cryo-electron microscopy. Cell 107:869–879

Reimer L (1997) Transmission electron microscopy, 4th edn. Springer, Berlin

Saibil HR (2006) Allosteri signaling of ATP hydrolysis in GroEL–GroES complexes. Nat Struct Mol Biol 13:147–152

Scherzer O (1949) The theoretical resolution limit of the electron microscope. J Appl Phys 20:20–29

Shimada A, Niwa H, Tsujita K, Suetsugu S, Nitta K, Suetsugu KH, Akasaka R, Nishino Y, Toyama M, Chen L, Liu ZJ, Wang BC, Yamamoto M, Terada T, Miyazawa A, Tanaka A, Sugano S, Shirouzu M, Nagayama K, Takenawa T, Yokoyama S (2007) Curved EFC/F-BAR-domain dimers are joined end to end into a filament for membrane invagination in endocytosis. Cell 129:761–772

Sieber P (1974) High resolution electron microscopy with heated apertures and reconstruction of single-sideband micrographs. In: Proceedings of the 8th international congress electron microscopy, vol 1. Academic Press, New York, pp 274–275

Smith FH (1947) Microscopes, British patent 639 014, Class 97(i) CroupXX

Stagg SM, Lander GC, Pulokas J, Fellmann D, Cheng A, Qulspe JD, Mallick SP, Avila RM, Crragher B, Potter CS (2006) Automated cryoEM data acquisition and analysis of 284742 particles of GroEL. J Struct Biol 155:470–481

Tonomura A, Osakabe N, Matsuda T, Kawasaki T, Endo J, Yano S, Yamada H (1986) Evidence for Aharonov–Bohm effect with magnetic field completely shielded from electron wave. Phys Rev Lett 56:792–795

Unwin PNT (1970) An electrostatic phase plate for the electron microsope. Bunsen-Ges 74:1137–1141

Van Harreveld A, Crowell J (1964) Electron microscopy after rapid freezing on a metal surface and substitution fixation. Anat Rec 149:381–386

Willash D (1975) High resolution electron microscopy with profiled phase plates. Optik 44:17–36

Yasuta H, Okawara H, Nagayama K (2006) Aharonov–Bohm phase plate in transmission electron microscopy. In: Proceedings of the 16th international microscope congress, vol 1. Japan Society of Microscopy, Sapporo, p 90, 7 Sept 2006

Zernike F (1942) Phase contrast, a new method for the microscopic observation of transparent objects. Physica 9:686–698, 974–986